

Stopping power of hot dense deuterium-tritium plasmas mixed with impurities to charged particles

Zhen-Guo Fu¹,[✉] Zhigang Wang,¹ Chongjie Mo^{2,1},[✉] Dafang Li,¹ Weijie Li,¹ Yong Lu,³
Wei Kang,⁴ Xian-Tu He,^{1,4} and Ping Zhang^{1,2,4,*}

¹*Institute of Applied Physics and Computational Mathematics, Beijing 100088, China*

²*Beijing Computational Science Research Center, Beijing 100193, China*

³*College of Mathematics and Physics, Beijing University of Chemical Technology, Beijing 100029, China*

⁴*HEDPS, Center for Applied Physics and Technology, Peking University, Beijing 100871, China*



(Received 25 December 2019; revised manuscript received 20 March 2020; accepted 12 May 2020;
published 26 May 2020)

In this work, we studied the stopping power of deuterium-tritium (DT) plasmas mixed with impurities to the injected charged particles. Based on the Brown-Preston-Singleton model, the analytical expression for the change ratio of stopping power (denoted by η) induced by impurities in DT plasmas is developed, in which both classical short-distance collision part and quantum correction contribution are purely linear response to the impurity concentration ξ_X , while the classical long-range collision brings about higher-order nonlinear response to ξ_X . Furthermore, the expression for change ratio of deposition depth (denoted by χ) of charged particles induced by impurities in DT plasmas is also derived. As applications, we systemically investigated the energy loss of α particles deposited into a hot dense DT plasma mixed with impurity X ($X = \text{C}, \text{Si}, \text{Ge}$), where the temperature and density of DT are smaller than 10 keV and 500 g/cm³ and the concentration of X ξ_X is less than 5%. The numerical results suggest that (i) for the case of C mixed into DT, both change ratios of stopping power and deposition depth of α particles (i.e., η and χ) are linear response to the concentration of C ξ_C ; (ii) for the case of Si mixed into DT, the second-order nonlinear response of η and χ to ξ_{Si} cannot be ignored when the densities of DT are larger than 200 g/cm³; and (iii) for the case of Ge mixed into DT, the second- and third-order nonlinear response of η and χ to ξ_{Ge} are very remarkable because of the higher ionization degree and heavier atomic mass of Ge. The formulas and findings in this work may be helpful to the research of internal confinement fusion (ICF) related implosion physics and may provide useful theoretical guidance and data for the design of ICF target.

DOI: [10.1103/PhysRevE.101.053209](https://doi.org/10.1103/PhysRevE.101.053209)

I. INTRODUCTION

High-energy projectiles, such as α particle, proton, and deuteron, created by fusion reactions deposit energy into the dense plasmas as they are stopped. How to accurately model the stopping power of plasmas to the charged particles is thus an interesting and important issue in modern internal confinement fusion (ICF) [1–6], astrophysics [7], condensed matter physics, and other research fields since the charged particle stopping power in low-temperature materials and high-temperature plasmas will strongly affect energy transport and heating in these fusion processes. Because of the importance from the perspectives of both basis physics and potential applications in the fields of high-energy-density physics, a series of theoretical models and advanced simulation methods for the stopping power have been developed. From the model-developing side, two main methods have been proposed to describe the interactions between injected charged particle and plasmas, i.e., the dielectric response formulation [8–11] and the collisional approach [12–17]. Based on the latter, for example, a popular model using a rigorous expansion in a

small parameter and dimensional continuation of collisional transport coefficients have been described by Brown, Preston, and Singleton (BPS) [13]. From the numerical simulation side, both classical molecular dynamics simulations and first-principle methods based on quantum mechanics have been developed. For the charged particle stopping power in weak- to moderately strong coupling plasmas, classical molecular dynamics simulations may provide excellent results [18]. While for the strong-coupling plasmas, in which the strong many-body coupling and quantum electron degeneracy effects play essential roles, first-principles methods [19–24] based on a quantum mechanical treatment of the electrons, such as fully *ab initio* computational scheme based on linear response time-dependent density-functional theory [20], and *ab initio* time-dependent orbital-free density-functional (TD-OF-DFT) theory [21,22], may predict more accurate charged particle stopping power. The most recent investigations showed that for α -particle stopping in warm and solid-density deuterium-tritium (DT) plasmas, the simulation results of stopping power obtained by *ab initio* TD-OF-DFT [21,22] might be lower about $\sim 25\%$ in comparison with stopping power models often used in the high-energy-density physics community [12,13,25]. Thus, the regimes of validity and application of present stopping power models need to be further established by the relevant experiments.

*Corresponding author: zhang_ping@iapcm.ac.cn

With the advanced development of high-energy laser facilities in the world, such as the OMEGA laser facility and the National Ignition Facility (NIF) in the USA and the PHELIX laser facility in Germany, there has been significant effort for measuring the energy deposition of charged particles penetrating through the high-energy-density plasmas. Recent experiments [26–28] revealed that the Li-Petrasso (LP) model [12] and the BPS model [13], which are considered from the aspect of binary collision, provide better descriptions of the ion stopping around the Bragg peak in the weakly coupled plasmas than other models. While the experiment on the stopping power of protons in a warm dense beryllium with solid density and electron temperature of tens of eV showed that the dielectric response stopping power models are excellent choices for moderately and strongly coupled plasmas [29]. Furthermore, most recent neutron time-of flight measurements of charged particle energy loss in ICF plasmas indicated accurate distinguish between the LP model and random phase approximation dielectric response stopping power model [30].

More and more ICF related experiments were also carried out to characterizing the high-energy-density plasma in ICF via the passage of charged particle beams. In particular, α particles generated from DT fusion ($D+T \rightarrow \alpha+n$) deposit their energy in the hot spot of ICF DT-fusion, thus causing the hot-spot temperature to rise sharply and the thermonuclear burn wave to propagate in the surrounding DT fuel. The stopping power of charged particles, therefore, is crucial for predicting ignition in the central hot ICF capsule. However, the DT hot-spot contamination from ablator materials, such as beryllium (Be) [31], copper-doped Be, silicon- (Si) doped plastic (CH) [32,33], germanium- (Ge) doped CH [34,35], and high-density carbon (HDC) [36–39], and the inner side of hohlraum materials [such as gold (Au) and U] [40] will significantly influence the energy deposition of α particles in the DT capsule and then result in DT neutron yield and ion temperature both decrease abruptly. Especially, Ge x-ray spectroscopy was initially used to infer the mix of targets with a Ge dopant CH layer in the ablator. Later, Ge was replaced by Si, which demonstrated improved radiation absorption and higher implosion velocity. Recently, a set of experiments demonstrated that the HDC ablator in a near-vacuum hohlraum is a viable candidate for achieving α -particle heating and ignition on the -. In recent years, we have theoretically studied the influence of Be and U on the stopping power of DT to charged particles [41,42]. However, there is little quantitative investigation about the effects of ablator materials, including C, Si, and Ge, on the stopping power of dense DT plasmas for α particle generated from DT fusion. Because of the basic interest and the presence of C, Si, and Ge in the ICF capsule, it is timely to provide a systematically theoretical analysis for the stopping power of DT plasmas mixed with C-Si-Ge to the α particle.

Here, by employing the BPS model [13], which has been experimentally demonstrated as an excellent model for weakly coupled plasmas, we study the influence of the impurities in DT plasmas on the energy loss of charged particle deposited therein. The analytical derivations of the change ratio of stopping power induced by impurities in DT plasmas reveal that (i) both classical short-distance collision

and quantum correction contributions linearly depend on the impurity concentration ξ_X , (ii) while the classical long-range collision contribution also leads to higher-order nonlinear response to ξ_X . The explicit expressions for the linear and nonlinear response coefficients are obtained. Furthermore, the expression for change ratio of deposition depth (denoted by χ) of charged particles induced by impurities in DT plasmas is also derived. Combined the analytical analysis and numerical simulations, we systemically study the stopping power of hot dense DT plasmas mixed with impurity X ($X = C, Si, Ge$) to α particles within high velocity. We find that when C is mixed into DT, both change ratios of stopping power and deposition depth of α particles (i.e., η and χ) are linear response to the concentration of C ξ_C ; while if Si (Ge) is mixed into DT, the second- (and even third-) order nonlinear responses of η and χ to ξ_{Si} (ξ_{Ge}) become significant. This is because of the higher ionization degrees and heavier atomic masses of Si and Ge. We hope our results should be helpful to the research of ICF related implosion physics and can provide useful theoretical guidance and data for the design of ICF target.

The paper is organized as follows. In Sec. II we introduce the BPS model and provide detailed derivations of change ratio of stopping power induced by impurities. In Sec. III, detailed discussions for the linear and nonlinear responses of η and χ to the concentration ξ_X of impurities X ($= C, Si, Ge$) mixed into DT plasmas. The paper is summarized and concluded in Sec. IV.

II. METHOD DESCRIPTIONS

In the following derivations, we assume that the plasma is temperature equilibrium that $\beta_e = \beta_D = \beta_T = \beta_X = \beta$, and the number densities of D and T satisfy the relationship that $n_D/n_T = m_T/m_D$, which results in the mass densities of D and T are equal to each other, i.e., $\rho_D = \rho_T$, and the number density of X is

$$n_X = \xi_X n_T, \quad (1)$$

where ξ_X is the mixing concentration of X ($= C, Si, Ge$). Due to the electric neutrality, the number density of electron is

$$\begin{aligned} n_e &= Z_D n_D + Z_T n_T + Z_X n_X \\ &= (1 + m_T/m_D + Z_X \xi_X) n_T, \end{aligned} \quad (2)$$

where $Z_D = Z_T = 1$.

The stopping power of nonrelativistic charged particles moving through a fully ionized plasma for Coulomb interaction is given by [13]

$$S(v_p) = S_s(v_p) + S_l(v_p) + S_q(v_p), \quad (3)$$

where the first term in the right-hand side of Eq. (3) represents classical short-distance contribution, which is written as

$$S_s(v_p) = \sum_b S_{b,s}(v_p) = \sum_b A_b I_b(v_p). \quad (4)$$

Here

$$A_b = \frac{Z_p^2 e^2 \kappa_b^2}{2\beta^2 m_p m_b v_p}, \quad (5)$$

where v_p is the projectile velocity, $Z_p e$ denotes the charge of projectile p , m_p (m_b) denote the mass of projectile p (plasma

species b), and

$$\kappa_b^2 = \beta Z_b^2 e^2 n_b \quad (6)$$

is the Debye wave number of plasma species b ($b = i, e$ denote ion and electron respectively) with n_b being the number density of species b . $I_0(v_p)$ in Eq. (4) is written as

$$I_b(v_p) = \int_0^1 du \sqrt{u} \{ -\ln [Bu/(1-u)] + 2(1-\gamma) \} \\ \times [\beta M_{pb} v_p^2 - 1/u] + 2/u) f(\sqrt{u} v_p), \quad (7)$$

where $B = \frac{\beta Z_p Z_b e^2 K}{4\pi} \frac{m_b}{m_{pb}}$ with K being an arbitrary wave number, $m_{pb} = \frac{m_p m_b}{m_p + m_b}$ and $M_{pb} = m_p + m_b$ are the reduced mass and the total mass of the projectile and plasma particles respectively, γ is the Euler's constant, and $f(v) = \left(\frac{\beta m_b}{2\pi}\right)^{\frac{3}{2}} e^{-\frac{\beta m_b v^2}{2}}$ is the Maxwell-Boltzmann distribution. In the following discussions, projectile p is considered as α particle, and plasma species b contain ions of D, T, X ($=$ C, Si, Ge) and electrons. From then on, Eq. (4) can be rewritten as

$$S_s(v_p) = \sum_{b \neq X} A_b I_b(v_p) + A_X I_X(v_p) \\ = \frac{(Z_p e^2)^2}{2\beta m_p v_p} \left[\sum_{b \neq X} \frac{Z_b^2 n_b}{m_b} I_b(v_p) + \frac{Z_X^2 \xi_X n_T}{m_X} I_X(v_p) \right]. \quad (8)$$

We define the change ratio of the classical short-distance contribution of stopping power of DT plasmas caused by X mixing as

$$\eta_s = \frac{S_s(v_p) - S_s^0(v_p)}{S_s^0(v_p)}, \quad (9)$$

where $S_s^0(v_p)$ is the classical short-distance contribution of stopping power of DT plasmas without mixing other materials. By using Eqs. (1), (2), and (8), one can easily get that

$$\eta_s = a_1 \xi_X, \quad (10)$$

where

$$a_1 = \frac{1}{U(v_p)} \left[\frac{Z_X I_e(v_p)}{m_e} + \frac{Z_X^2 I_X(v_p)}{m_X} \right] \quad (11)$$

with $U(v_p) = \frac{m_T}{m_D} I_D(v_p) + \frac{1}{m_T} I_T(v_p) + \frac{m_D + m_T}{m_D m_e} I_e(v_p)$. It is clear that η_s is independent of the densities of DT plasmas but purely linear response to the mixing concentration ξ_X .

While the second term in the right-hand side of Eq. (3) describes the long-distance contribution, which may be given

by

$$S_l(v_p) = \sum_b S_{b,l}(v_p) \\ = \left(\frac{Z_p e}{2\pi} \right)^2 \sum_b \left\{ \frac{\text{Im}[G_b(v_p)]}{\beta m_p v_p^2} - \frac{1}{2} \int_{-1}^1 dss \text{Im}[G_b(sv_p)] \right\}, \quad (12)$$

where $s = \cos \theta$ with the angle θ being the relative angle between the wave vector in the dielectric function and the velocity \mathbf{v}_p , and

$$G_b(z) = \frac{\rho_b(z)}{\rho_{\text{tot}}(z)} F(z) \ln[F(z)/K^2], \quad (13)$$

with $\rho_b(z) = \frac{2\pi \kappa_b^2 z}{\beta m_b} f(z)$ being an odd function related to the Maxwell-Boltzmann distribution,

$$\rho_{\text{tot}}(z) = \sum_c \rho_c(z) = \rho_{\text{tot}}^0(z) + \tilde{\rho}_X(z), \quad (14)$$

being the spectral weight. Here $\rho_{\text{tot}}^0(z) = \sum'_c \rho_c(z)$ with the superscript ' denoting the summation of DT plasmas without mixing with other materials and

$$\tilde{\rho}_X(z) = \frac{2\pi e^2}{m_X} (Z_X + Z_X^2) \xi_X n_T f(z) z. \quad (15)$$

Furthermore,

$$F(z) = \sum_d \kappa_d^2 J_d(z) = F_0(z) + \tilde{F}_X(z), \quad (16)$$

where $J_d(z) = 1 - \frac{4\pi^{3/2}}{\beta m_d} (z \int_0^\epsilon dt e^{t^2} - i \frac{\sqrt{\pi}}{2}) f(z)$ with $\epsilon = \sqrt{\frac{\beta m_d}{2}} z$, $F_0(z) = \sum'_d \kappa_d^2 J_d(z)$, and

$$\tilde{F}_X(z) = [Z_X^{-1} J_e(z) + J_X(z)] \kappa_X^2 \\ = [Z_X^{-1} J_e(z) + J_X(z)] \beta Z_X^2 e^2 n_T \xi_X. \quad (17)$$

And then, let us derive the change of classical long-distance contribution of stopping power of DT plasmas caused by X mixing, which is given by

$$S_l(v_p) - S_l^0(v_p) = \left(\frac{Z_p e}{2\pi} \right)^2 \left[\frac{\text{Im}(\sum_b G_b - \sum'_b G_b^0)}{\beta m_p v_p^2} \right. \\ \left. - \frac{1}{2} \text{Im} \int_{-1}^1 dss (\sum_b G_b - \sum'_b G_b^0) \right], \quad (18)$$

where $S_l^0(v_p)$ is the classical long-range contribution of stopping power of DT plasmas without mixing other materials, and

$$\sum_b G_b - \sum'_b G_b^0 = [F_0 + \tilde{F}_X] \ln \left(\frac{F_0 + \tilde{F}_X}{K^2} \right) - F_0 \ln \left(\frac{F_0}{K^2} \right). \quad (19)$$

We also define

$$\eta_l = \frac{S_l(v_p) - S_l^0(v_p)}{S_l^0(v_p)}. \quad (20)$$

Substituting Eqs. (17)–(19) into Eq. (20), we can clearly find that η_l is not purely linear response to ξ_X , which differs from the short-distance term η_s . By performing the Taylor’s series expansion to the limit of $\xi_X \rightarrow 0$, we get that

$$\eta_l = \frac{1}{\Lambda_0(v_p)} \left[\text{Im} \left(\{1 + \ln[F_0(v_p)/K^2]\} \tilde{F}_X(v_p) + \frac{\tilde{F}_X^2(v_p)}{2F_0(v_p)} - \frac{\tilde{F}_X^3(v_p)}{6F_0^2(v_p)} + \dots \right) - \frac{1}{2} \int_{-1}^1 ds \text{Im} \left(\{1 + \ln[F_0(sv_p)/K^2]\} \tilde{F}_X(sv_p) + \frac{\tilde{F}_X^2(sv_p)}{2F_0(sv_p)} - \frac{\tilde{F}_X^3(sv_p)}{6F_0^2(sv_p)} + \dots \right) \right], \quad (21)$$

where

$$\Lambda_0(v_p) = \text{Im}\{F_0(v_p) \ln[F_0(v_p)/K^2]\} - \frac{1}{2} \int_{-1}^1 ds \text{Im}\{F_0(sv_p) \ln[F_0(sv_p)/K^2]\}. \quad (22)$$

And then the linear response to ξ_X is explicitly given by

$$\eta_l(\xi_X \rightarrow 0) = b_1 \xi_X. \quad (23)$$

where

$$b_1 = \beta Z_X^2 e^2 n_T \frac{\text{Im}[\Gamma_1(v_p)] - \frac{1}{2} \int_{-1}^1 ds \text{Im}[\Gamma_1(sv_p)]}{\Lambda_0(v_p)} \quad (24)$$

with

$$\Gamma_1(z) = \{1 + \ln[F_0(z)/K^2]\} [Z_X^{-1} J_e(z) + J_X(z)]. \quad (25)$$

In contrast to η_s , η_l is related to the density of DT plasma n_T , which is implicitly included in $F_0(v_p)$ as well as logarithm functions in Eqs. (21) and (24). In addition, the nonlinear response to ξ_X induced by high-order terms of $\tilde{F}_X(z)$ in Eq. (21) may become of importance for larger mixing concentration ξ_X as well as larger degree of ionization Z_X . Combining the short-distance contribution and long-range contribution of stopping power, the linear response of classical part of stopping power to the mixing concentration ξ_X could be easily obtained as

$$\eta_{cl} = \frac{a_1 S_s^0(v_p) + b_1 S_l^0(v_p)}{S_s^0(v_p) + S_l^0(v_p)} \xi_X. \quad (26)$$

The last term in Eq. (3) is the quantum correction to the classical part, which is written as

$$S_q(v_p) = \sum_b A_b Q_b(v_p), \quad (27)$$

where

$$Q_b(v_p) = \frac{1}{v_p} \int_0^\infty dv_{pb} [\text{Re} \psi(1 + i\eta_{pb}) - \ln \eta_{pb}] \times \{[1 + \alpha_-] f_M(v_-) - [1 + \alpha_+] f_M(v_+)\}. \quad (28)$$

Here $\psi(z) = \frac{d \ln \Gamma(z)}{dz}$ is the logarithmic derivative of the gamma function, $\eta_{pb} = \frac{Z_p Z_b e^2}{4\pi \hbar v_{pb}}$ with \hbar the Planck constant, $v_\pm = v_p \pm v_{pb}$ with $v_{pb} = |\mathbf{v}_p - \mathbf{v}_b|$ being the relative velocity, and $\alpha_\pm = \frac{M_{pb}}{m_b} \frac{v_p}{v_{pb}} (\frac{1}{\beta m_b v_p v_{pb}} \pm 1)$. This calculation is exact to leading and next-to-leading order in the plasma coupling parameter, including an exact treatment of two-body quantum scattering [13]. Similarly to η_s shown in Eq. (9), we define the change ratio of the quantum correction term of stopping

power of DT plasmas caused by X mixing as follows:

$$\eta_q = \frac{S_q(v_p) - S_q^0(v_p)}{S_q^0(v_p)}, \quad (29)$$

where $S_q^0(v_p)$ is the quantum part of stopping power of DT plasmas without mixing other materials. After some simple algebraic operations, we have

$$\eta_q = c_1 \xi_X, \quad (30)$$

where

$$c_1 = \frac{1}{W(v_p)} \left[\frac{Z_X Q_e(v_p)}{m_e} + \frac{Z_X^2 Q_X(v_p)}{m_X} \right] \quad (31)$$

with $W(v_p) = \frac{m_T}{m_D} Q_D(v_p) + \frac{1}{m_T} Q_T(v_p) + \frac{m_D + m_T}{m_D m_e} Q_e(v_p)$, which is formally consistent with η_s above. Therefore, η_q is also independent of the densities of DT plasmas but directly proportional to ξ_X . Finally, the change ratio of the total stopping power due to the mixing of X ,

$$\eta = \frac{S(v_p) - S^0(v_p)}{S^0(v_p)}, \quad (32)$$

is derived as follows:

$$\eta = \frac{\eta_s S_s^0(v_p) + \eta_l S_l^0(v_p) + \eta_q S_q^0(v_p)}{S^0(v_p)} = \alpha_1 \xi_X + \alpha_2 \xi_X^2 + \alpha_3 \xi_X^3 + \dots, \quad (33)$$

where $S^0(v_p) = S_s^0(v_p) + S_l^0(v_p) + S_q^0(v_p)$, and the linear response coefficient to ξ_X is analytically given by

$$\alpha_1 = \frac{a_1 S_s^0(v_p) + b_1 S_l^0(v_p) + c_1 S_q^0(v_p)}{S^0(v_p)}. \quad (34)$$

The nonlinear response to ξ_X is derived from the long-range contributions of the stopping power. Explicitly,

$$\alpha_2 = \frac{S_l^0(v_p)}{S^0(v_p)} b_2, \quad (35)$$

$$\alpha_3 = \frac{S_l^0(v_p)}{S^0(v_p)} b_3, \quad (36)$$

where

$$b_2 = \frac{(\beta Z_X^2 e^2 n_T)^2 \{ \text{Im}[\Gamma_2(v_p)] - \frac{1}{2} \int_{-1}^1 ds \text{Im}[\Gamma_2(sv_p)] \}}{\Lambda_0(v_p)}, \quad (37)$$

$$b_3 = \frac{(\beta Z_X^2 e^2 n_T)^3 \{ \text{Im}[\Gamma_3(v_p)] - \frac{1}{2} \int_{-1}^1 ds \text{Im}[\Gamma_3(sv_p)] \}}{\Lambda_0(v_p)}, \quad (38)$$

with

$$\Gamma_2(z) = \frac{[Z_X^{-1}J_e(z) + J_X(z)]^2}{2F_0(z)}, \quad (39)$$

$$\Gamma_3(z) = -\frac{[Z_X^{-1}J_e(z) + J_X(z)]^3}{6F_0^2(z)}. \quad (40)$$

The deposition distance of projected particles in plasmas is given by

$$r(E, E_0, \xi_X) = \int_E^{E_0} dE' S^{-1}(E'), \quad (41)$$

where E_0 is the initial energy of the α particle which is chosen as the DT reaction energy ($E_0 = 3.54$ MeV) in the following calculations, and E is the energy of the system. In the following discussions, we also pay close attention to the linear response of the change of $r(E; E_0)$ to the mixing concentration ξ_X of ablator materials X . For this purpose, we introduce the change ratio of the deposition distance

$$\chi = \frac{r(E, E_0, \xi_X = 0) - r(E, E_0, \xi_X)}{r(E, E_0, \xi_X = 0)} = \frac{r_0 - r}{r_0}, \quad (42)$$

where $r_0 = r(E, E_0, \xi_X = 0) = \int_E^{E_0} dE' \frac{1}{S^0(E')}$. Substituting Eq. (33) into Eqs. (41) and (42) and carrying out the Taylor's series expansion to the limit of $\xi_X \rightarrow 0$, we have

$$\begin{aligned} \chi(\xi_X \rightarrow 0) &= r_0^{-1} \int_E^{E_0} dE' \frac{\eta(E')}{[1 + \eta(E')]S^0(E')} \\ &= \gamma_1 \xi_X + \gamma_2 \xi_X^2 + \gamma_3 \xi_X^3 + \dots, \end{aligned} \quad (43)$$

where the linear and nonlinear response coefficients are given by

$$\gamma_1 = r_0^{-1} \int_E^{E_0} dE' \frac{\alpha_1(E')}{S^0(E')}, \quad (44)$$

$$\gamma_2 = r_0^{-1} \int_E^{E_0} dE' \frac{\alpha_2(E') - \alpha_1^2(E')}{S^0(E')}, \quad (45)$$

$$\gamma_3 = r_0^{-1} \int_E^{E_0} dE' \frac{\alpha_1^3(E') - 2\alpha_1(E')\alpha_2(E') + \alpha_3(E')}{S^0(E')}. \quad (46)$$

It is distinct that γ_i ($i = 1, 2, 3, \dots$) could be easily obtained once the coefficients α_i ($i = 1, 2, 3, \dots$) are known. The formulas of α_i and γ_i are useful and important for understanding the material-mixing rules in ICF plasmas and thereby may have advantages in the ICF target design.

III. NUMERICAL RESULTS FOR DT + C, Si, AND Ge

In our calculations, the densities of both D and T plasmas $\rho_{D,T}$ are assumed changing from ~ 1 g/cm⁻³ to ~ 500 g/cm⁻³, which corresponds to the number densities of D $n_D = 3 \times 10^{23} \sim 1.5 \times 10^{26}$ cm⁻³ and the number densities of T $n_T = 2 \times 10^{23} \sim 1.0 \times 10^{26}$ cm⁻³, respectively. The maximal concentration is taken as $\xi_X^{\max} = 5\%$ in all calculations. The temperature we considered is high enough ($T = 5$ – 10 keV) that the DT + X plasmas are fully ionized [43]. This temperature condition is easily achieved in present ICF experiments [44]. In order to explicitly verify the appropriation of the BPS model for the plasma conditions considered herein,

we carefully check the overall coupling of the projectile to the plasma, which is written as [13]

$$g_p^2 = \sum_b \beta^2 \left(\frac{e_p e_b}{4\pi} \right)^2 \kappa_b^2, \quad (47)$$

where $e_p = Z_p e$ is the charge of projectile, $e_b = Z_b e$ is the charge of plasma species labeled by b , and $\kappa_b = \sqrt{\beta n_b} e_b$ is the Debye wave number of species b . In the following calculations, we focus on the stopping power of hot dense DT + X ($X = \text{C, Si, Ge}$) plasmas to the projected α particle. Therefore, the coupling strength of the α particle to the DT + X ($X = \text{C, Si, Ge}$) plasmas are calculated. Typical results of g_p as a function of density and temperature of DT plasma are shown in Fig. 1. As mentioned above, the density of DT plasma changes from ~ 1 g/cm³ to ~ 500 g/cm³ and the temperature of DT plasma changes from ~ 5 keV to ~ 10 keV. Figures 1(a) and 1(b) are for the cases of DT + C with the mixing concentrations $\xi_C = 2\%$ and $\xi_C = 5\%$, respectively; Figs. 1(c) and 1(d) are for the cases of DT + Si with $\xi_{\text{Si}} = 2\%$ and $\xi_{\text{Si}} = 5\%$, respectively; while Figs. 1(e) and 1(f) are for the cases of DT + Ge with $\xi_{\text{Ge}} = 2\%$ and $\xi_{\text{Ge}} = 5\%$, respectively. Since g_p is directly proportional to $n_b^{1/2}$ and inversely proportional to $T^{3/2}$, we can see from Fig. 1 that g_p increases with increasing the density of DT but decreases with increasing the temperature of plasma. For the plasma conditions that $\rho_{D,T} = 500$ g/cm³, $T = 5$ keV, and $\xi_X = 5\%$ ($X = \text{C, Si, Ge}$), the maximum values of g_p are 0.051 for DT + C plasma, 0.16 for DT + Si plasma, and 0.51 for DT + Ge plasma, see Figs. 1(b), 1(d), and 1(f), respectively. Therefore, the DT + X ($X = \text{C, Si, Ge}$) plasmas studied herein are weakly coupled, which verifies that the BPS method is appropriate [13]. Furthermore, as mentioned in Ref. [13], the DT + X plasmas studied in this work are composed of nonrelativistic particles that have no degeneracy. Based on these plasma conditions, we first performed the fundamentally numerical calculations by employing the Eqs. (32) and (42) based on the BPS model, and then the formulas of α_i and γ_i shown above are considered to intensively explore the linear and nonlinear response effects induced by the mixed materials.

A. DT + C plasmas

We first discuss the influence of C mixing into the hot dense DT plasmas. Some numerical results of η [Eq. (32)] as a function of the incident energy of α -particle E_α ($E_\alpha = \frac{1}{2} m_p v_p^2$) are shown in Fig. 2. Here, the temperature of plasma system is chosen as $T = 5$ keV, and a typical mixing concentration of C is considered that $\xi_C = 2\%$. Different data symbols in Fig. 2 correspond to different densities of DT plasmas. Explicitly, black squares, red circles, green triangles, and blue stars in Fig. 2 are for $\rho_D = \rho_T = 5, 10, 50,$ and 100 g/cm³, respectively. The change ratios of total, classical part, and quantum correction of stopping powers are presented in Fig. 2(a), Fig. 2(b), and Fig. 2(c), respectively. From Fig. 2(a) we can see that with increasing the incident energy of α -particle E_α , the change ratio of total stopping power η (induced by C mixing) gradually decreases and then slowly increases. When the energy of α -particle E_α exceeds about ~ 5 MeV, η reaches a saturation value, hardly varying with E_α . Same as total stopping power, the change ratio of classical part of stopping

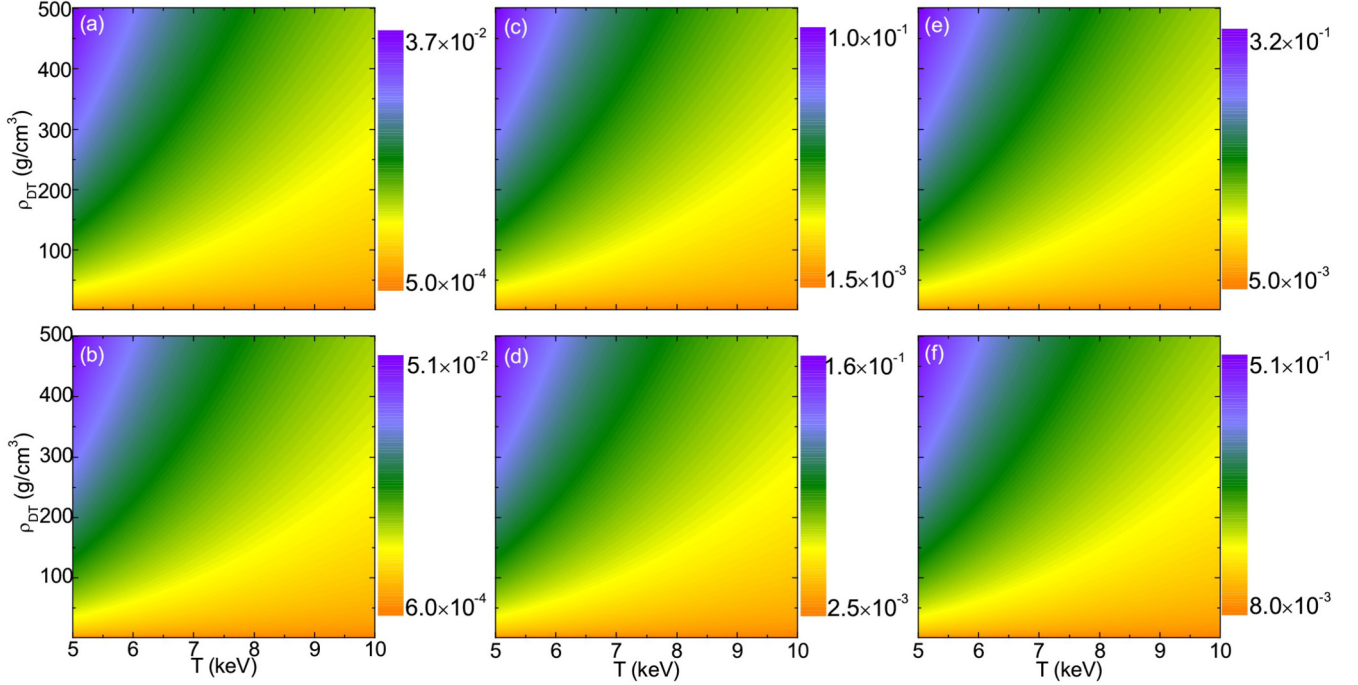


FIG. 1. Overall coupling strength g_p of the projected α particle to the DT + X ($X = C, Si,$ and Ge) plasmas as a function of temperature T (in unit of keV) and density ρ_{DT} (in unit of g/cm^3) of DT. Panels (a) and (b) are for the case of DT + C with $\xi_C = 2\%$ and $\xi_C = 5\%$, panels (c) and (d) are for the case of DT + Si with $\xi_{Si} = 2\%$ and $\xi_{Si} = 5\%$, and panels (e) and (f) are for the case of DT + Ge with $\xi_{Ge} = 2\%$ and $\xi_{Ge} = 5\%$.

power, i.e., η_{cl} , also exhibits the same variation pattern with the incident energy of α particle, which is shown in Fig. 2(b).

Remarkably differing from η and η_{cl} , the change ratio of quantum correction part of stopping power, i.e., η_q , is independent of the density of DT plasmas, which could be found from analytical expressions (29)–(31). Therefore, we just observe one black squares in Fig. 2(c), and other three (red circles, green triangles, and blue stars) are overlapped with the black squares. Moreover, we see from Fig. 2(c) that when the energy of α -particle E_α is small, η_q tends to zero and rises rapidly with increasing E_α . This is because that when the incident velocity of α particle is small, the quantum Coulomb parameter η_{pb} in Eq. (28) is large so that the scattering is nearly dominated by the classical scattering. However, when

E_α is far greater than the system temperature T , η_q no longer changes with E_α , see Fig. 2(c). This is because that when $E_\alpha \rightarrow \infty$, following from Eq. (30), η_q could be approximated as a simple expression that

$$\eta_q(E_\alpha \rightarrow \infty) \approx \frac{m_D}{m_D + m_T} Z_x \xi_X. \quad (48)$$

Explicitly, for the case of $\xi_C = 2\%$ and $Z_C = 6$, we could immediately obtain that $\eta_q(E_\alpha \rightarrow \infty) \approx 4.8$, which is well consistent with the numerical result shown in Fig. 2(c).

In addition, from this asymptotic expression (48), we get that (i) for the case of C mixing into DT plasmas with $\xi_C = 0.6\%$, and 5.0% , $\eta_q(E_\alpha \rightarrow \infty) \approx 1.44\%$, and 12.0% ; (ii) for the case of Si mixing into DT plasmas with $Z_{Si} = 14$ and

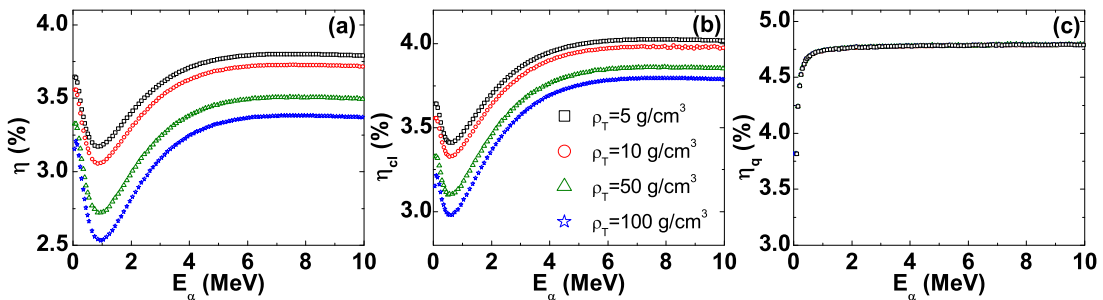


FIG. 2. Change ratio of stopping power of DT plasmas mixed with carbon to α particle as a function of the incident energy of α -particle E_α . (a) For the total stopping power, (b) for the classical part of stopping power, and (c) for the quantum part of stopping power. Different data symbols are for different densities of T, i.e., black squares, red circles, green triangles, and blue stars correspond to $\rho_T = 5, 10, 50,$ and $100 g/cm^3$, respectively. The temperature of plasma is chosen as $T = 5$ keV, the carbon mixing concentration is $\xi_C = 2\%$, and the density of D is chosen as $\rho_D = \rho_T$.

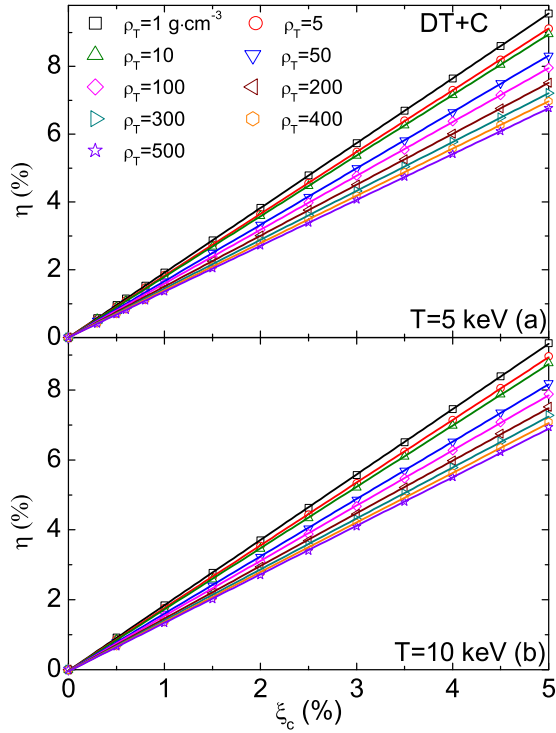


FIG. 3. Change ratio of stopping power of DT + C plasmas to α particle as a function of the C-mixing concentration ξ_C . Various densities of DT plasmas are considered that $\rho_D = \rho_T = 1, 5, 10, 50, 100, 200, 300, 400,$ and 500 g/cm^3 , and the temperature of plasmas is chosen as $T = 5 \text{ keV}$ in (a) and $T = 10 \text{ keV}$ in (b), respectively. Discrete symbols are calculated via Eq. (32), while the color lines are calculated via Eq. (33) where just linear term $\sim \alpha_1 \xi_C$ is taken into account. The initial energy of α particle is chosen as $E_0 = 3.54 \text{ MeV}$.

$\xi_{\text{Si}} = 0.6\%$, and 5.0% , $\eta_q(E_\alpha \rightarrow \infty) \approx 3.36\%$, and 28.0% ; and (iii) for the case of Ge mixing into DT plasmas with $Z_{\text{Ge}} = 32$ and $\xi_{\text{Ge}} = 0.6\%$, and 5.0% , $\eta_q(E_\alpha \rightarrow \infty) \approx 7.68\%$, and 64.0% . These approximation results are all in good agreement with the accurately numerical calculations, which are not shown for brevity.

In order to extract the relationship between η and ξ_C , we perform a series of calculations of stopping power of α particle with initial energy $E_0 = 3.54 \text{ MeV}$ moving in the DT + C plasmas with various densities that $\rho_D = \rho_T = 1, 5, 10, 50, 100, 200, 300, 400,$ and 500 g/cm^3 and two temperatures $T = 5$ and 10 keV . Firstly, by using the BPS model, we calculate the stopping powers $S(v_p)$ and $S^0(v_p)$ for DT + C plasmas and pure DT plasmas, and substitute the results into Eq. (32) to get the change ratio of stopping power induced by C mixing. The results are presented by discrete symbols in Fig. 3, where different shape symbols correspond to different densities of DT. Figures 3(a) and 3(b) are for the temperature $T = 5$ and 10 keV , respectively. These plasma conditions are easily realized in the modern ICF implosion experiments. Secondly, by employing Eqs. (33) and (34), we obtain the linear response term of η to ξ_C , which are plotted by color lines in Fig. 3. It is clear that the lines are in good agreement with the symbols, which indicate that the change ratio of stopping power of DT plasmas mixed with C to α particles is linear response to the concentration ξ_C . We emphasize again that the maximal concentration is taken as $\xi_C^{\text{max}} = 5\%$ in our calculations. The linear response rule that $\eta = \alpha_1 \xi_C$ found here may be of interest and importance for understanding the implosion physics as well as hydrodynamic instability in ICF related experiments, and may be also useful for the design of ICF capsule with HDC ablator layer. The linear coefficient α_1 for each line in Fig. 3 are summarized in Table I. We can see from Table I that α_1 decreases with increasing the density of DT plasmas. Furthermore, the maximal change ratio of stopping power induced by C mixing reaches about $\sim 8.5\%$, see Fig. 3. Comparing the results in Figs. 3(a) and 3(b), we find that η seems insensitive to the temperature, which could also be seen from the data of α_1 shown in Table I. In addition, if the concentration ξ_C is much larger than 5% , the quadratic- and even cubic-type nonlinear responses to ξ_C may become non-negligible (not shown for brevity).

Figure 4 presents the change ratio of deposition depth χ of an α particle with initial energy $E_0 = 3.54 \text{ MeV}$ injected in DT + C plasmas with various densities of DT. Similar to the treatment of stopping power shown in Fig. 3, the discrete symbols in Fig. 4 are the results calculated by using

TABLE I. The coefficients $\alpha_1, \alpha_2,$ and α_3 obtained by Eqs. (33)–(40) for DT+X ($X = \text{C, Si, and Ge}$) plasmas with various densities of DT that $\rho_D = \rho_T = 1, 5, 10, 50, 100, 200, 300, 400,$ and 500 g/cm^3 and two temperatures $T = 5$ and 10 keV . The values of $\alpha_1, \alpha_2,$ and α_3 listed in this table correspond to the color curves shown in Fig. 2 for the DT+C case, Fig. 4 for the DT+Si case, and Fig. 6 for the DT+Ge case.

ρ_T (g/cm^3)	DT+C		DT+Si				DT+Ge					
			5 keV		10 keV		5 keV			10 keV		
	α_1	α_1	α_1	α_2	α_1	α_2	α_1	α_2	α_3	α_1	α_2	α_3
1.0	1.91	1.87	4.04	–	4.05	0.040	6.44	0.829	–0.072	8.60	0.718	–0.062
5.0	1.82	1.79	3.77	–	3.82	0.045	5.32	0.959	–0.084	7.84	0.816	–0.071
10.0	1.79	1.75	3.63	–	3.69	0.048	4.72	1.029	–0.089	7.44	0.866	–0.075
50.0	1.66	1.64	3.21	–	3.34	0.057	2.93	1.239	–0.108	6.30	1.012	–0.088
100.0	1.59	1.57	2.97	–	3.15	0.061	1.91	1.358	–0.119	5.68	1.092	–0.095
200.0	1.50	1.50	2.68	–	2.92	0.066	0.67	1.503	–0.131	4.95	1.184	–0.103
300.0	1.44	1.46	2.33	0.032	2.77	0.070	–0.18	1.603	–0.138	4.46	1.247	–0.109
400.0	1.39	1.42	2.16	0.033	2.65	0.072	–0.77	1.630	–0.140	4.09	1.295	–0.113
500.0	1.35	1.38	2.02	0.034	2.56	0.074	–1.44	1.749	–0.153	3.77	1.334	–0.117

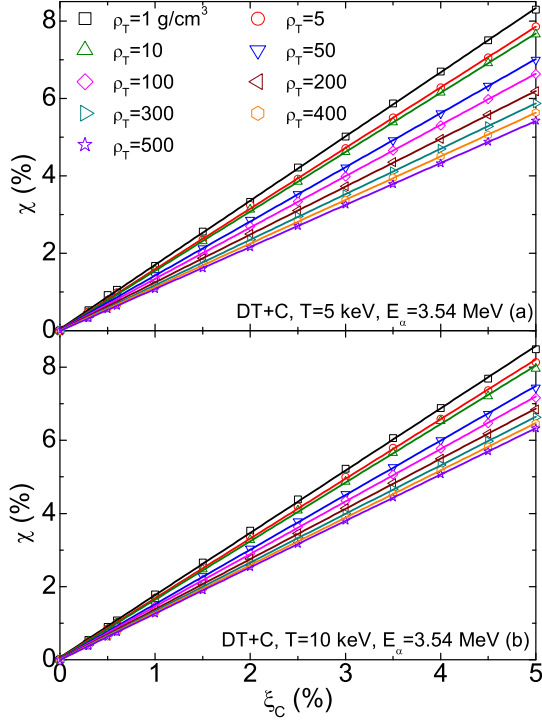


FIG. 4. Change ratio of deposition depth of α particle moving in the DT + C plasmas as a function of the C-mixing concentration ξ_C . (a) for the temperature of plasmas $T = 5$ keV, and (b) for $T = 10$ keV, respectively. Discrete symbols are calculated via Eq. (42), while the color lines are calculated via Eqs. (43) and (44) where just linear term $\sim \gamma_1 \xi_C$ is taken into account. Other parameters are the same as those used in Fig. 3.

Eq. (42), and the color lines are the results calculated by Eqs. (43) and (44) where only linear term of ξ_C is taken into account. The maximal change ratio of deposition depth induced by C mixing reaches about $\sim 8.5\%$. It is clear that for the small mixing concentration ($\xi_C \ll 5\%$) the change ratio of deposition depth of an α particle induced by C mixing could be well described by a linear response term $\chi = \gamma_1 \xi_C$. This conclusion is reasonable in wide ranges of density of

DT (from 1 g/cm^3 to 500 g/cm^3) and temperature (from 5 to 10 keV). The corresponding data of linear coefficient γ_1 are presented in Table II. It is seen from Table II that, same as α_1 shown in Table I, the smaller the density of DT, the greater the first-order coefficient γ_1 . This is because that γ_1 is directly proportional to the integral of α_1 .

B. DT + Si plasmas

Now let us turn to discuss the energy loss of α particle deposited into DT mixed with Si plasmas. For the sake of data integrity and for the convenience of comparative analysis with the case of DT + C, a series of numerical calculations are performed for DT + Si plasmas using the same parameters as in Figs. 3 and 4. Here, the degree of ionization of Si is $Z_{\text{Si}} = 14$ and the atomic effective mass of Si is $m_{\text{Si}} = 28.086$, which are larger than those of C. The results of η as a function of ξ_{Si} are illustrated in Fig. 5, in which Fig. 5(a) is for the case of $T = 5$ keV and Fig. 5(b) is for the case of $T = 10$ keV, respectively. It is obvious that the maximal change ratio of stopping power induced by Si mixing is larger than $\sim 20\%$. Following the same way treated to DT + C plasmas, we compare the results of the completely numerical calculation of the BPS model (the discrete symbols in Fig. 5) with the results obtained from the formulas (33)–(36) of linear and/or nonlinear response to mixing concentration ξ_{Si} (the color curves in Fig. 5). Unlike the case of DT + C, we find that when Si is mixed into DT plasmas, the quadratically nonlinear response of η to ξ_{Si} will gradually become significant as increasing the density and temperature of DT. For examples, we find that (i) at a temperature of 5 keV and DT density greater than 200 g/cm^3 , the quadratic term cannot be ignored, see Fig. 5(a); and (ii) at a temperature of 10 keV and DT density changing from 1 g/cm^3 to 500 g/cm^3 , the quadratic term is needed in order to predict more precise results, see Fig. 5(b). For much clearer understanding these analysis, the corresponding data of the first- and second-order coefficients α_1 and α_2 are presented in Table I. We can see that when $T = 5$ keV ($T = 10$ keV) and $\rho_T \geq 300 \text{ g/cm}^3$ ($\rho_T \geq 1 \text{ g/cm}^3$), α_2 becomes larger than ~ 0.032 (~ 0.040). Furthermore, the linear response coefficient α_1 for DT + Si plasmas is about 2 times larger than that

TABLE II. The coefficients γ_1 , γ_2 , and γ_3 obtained by Eqs. (44)–(46) for DT+X ($X = \text{C, Si, and Ge}$) plasmas with various densities of DT that $\rho_D = \rho_T = 1, 5, 10, 50, 100, 200, 300, 400,$ and 500 g/cm^3 and two temperatures $T = 5$ and 10 keV. The values of γ_1 , γ_2 , and γ_3 listed in this table correspond to the color curves shown in Fig. 3 for the DT+C case, Fig. 5 for the DT+Si case, and Fig. 7 for the DT+Ge case.

ρ_T (g/cm^3)	DT+C		DT+Si				DT+Ge					
			5 keV		10 keV		5 keV			10 keV		
	γ_1	γ_1	γ_1	γ_2	γ_1	γ_2	γ_1	γ_2	γ_3	γ_1	γ_2	γ_3
1.0	1.66	1.70	3.39	–	3.73	–0.032	8.75	–0.076	–0.048	10.56	–0.371	–0.031
5.0	1.57	1.63	3.11	–	3.51	–0.026	7.72	0.109	–0.074	9.88	–0.175	–0.049
10.0	1.53	1.60	3.05	–	3.26	0.002	7.38	0.190	–0.064	9.51	–0.059	–0.060
50.0	1.40	1.49	2.73	–	2.96	0.019	5.65	0.733	–0.121	8.54	0.195	–0.082
100.0	1.33	1.44	2.55	–	2.67	0.020	4.82	0.912	–0.134	7.92	0.398	–0.103
200.0	1.24	1.37	2.27	–	2.51	0.056	3.52	1.283	–0.169	7.04	0.646	–0.126
300.0	1.17	1.33	1.81	0.072	2.34	0.069	2.98	1.339	–0.170	6.84	0.701	–0.131
400.0	1.13	1.29	1.64	0.082	2.21	0.079	2.39	1.471	–0.181	6.51	0.794	–0.139
500.0	1.09	1.26	1.50	0.086	2.11	0.087	1.88	1.584	–0.190	6.22	0.871	–0.146

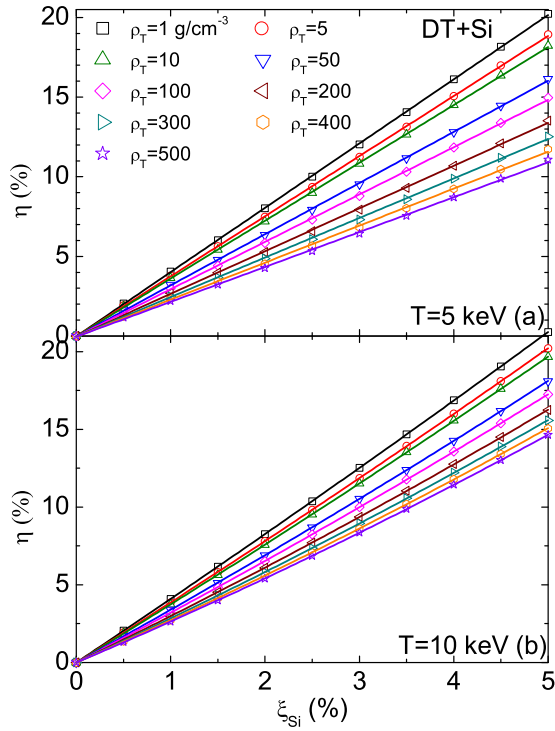


FIG. 5. Change ratio of stopping power of DT + Si plasmas to α particle as a function of the Si-mixing concentration ξ_{Si} . All other parameters are the same as those used in Fig. 3.

of DT + C plasmas. In addition, we find that with increasing the density of DT, the linear coefficient α_1 decreases while the second-order coefficient α_2 increases, which indicates the enhancement of the nonlinear response effect.

As mentioned above, similarly to Fig. 4, we exhibit in Fig. 6 the results of change ratio of deposition depth of α particle moving in DT + Si plasmas. The initial energy E_0 of α particle is still chosen as 3.54 MeV. All parameters are the same as those used in Fig. 5. After a variety of careful calculations, we find the second-order term of ξ_{Si} is necessary to provide more accurate results for higher densities and temperatures of DT plasmas, which is consistent with the analysis for stopping powers shown in Fig. 5. This could be clearly seen from Fig. 6 as well as the data of γ_1 and γ_2 for DT + Si shown in Table II. The same as the behaviors of α_1 and α_2 shown in Table I, with increasing the density of DT, the linear coefficient γ_1 decreases while the second-order coefficient γ_2 increases. Moreover, the maximal change ratio of χ induced by Si is more than 17%. Compared with the case of DT mixed with C, we can draw the following conclusion: Due to larger atomic mass of Si, the mixing of Si into the DT plasmas does cause a more significant decrease in the deposition depth of charged particle, but at the same time it will also result in higher-order nonlinear response of variation of deposition depth to Si mixing concentration.

C. DT + Ge plasmas

In this subsection, we will discuss the stopping power of DT + Ge plasmas to α particles. We know that C, Si, and Ge are all in the fourth main group of the periodic table. Because of the same number of electrons in their outermost shell,

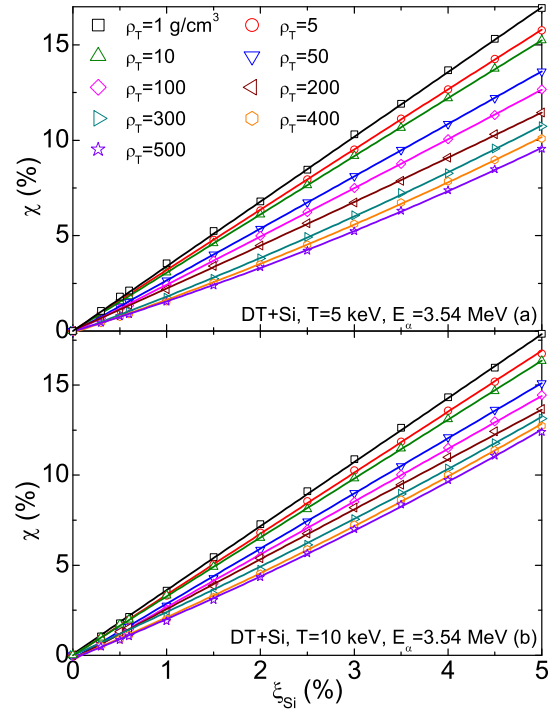


FIG. 6. Change ratio of deposition depth of α particle moving in DT + Si plasmas as a function of the Si-mixing concentration ξ_{Si} . All other parameters are the same as those used in Fig. 4.

their chemical properties are similar. This may be one of the reasons why C, Si, and Ge were used in the ICF target design [32–39]. Therefore, it is necessary for us to carefully analyze the influence of Ge mixed into the hot dense DT plasmas on the stopping power. We suppose Ge is fully ionized, i.e., $Z_{\text{Ge}} = 32$, when the temperature is higher than 5 keV.

The results of change ratio of stopping power induced by Ge mixed into DT are shown in Fig. 7. Similarly to the cases of DT + C and DT + Si shown in Figs. 3 and 5, the color curves shown in Fig. 7 are the results obtained from the formulas (33)–(36) which are truncated to the third-order nonlinear terms, while the discrete symbols are the results obtained from Eq. (32). The curves agree very well with the discrete symbols. It can be seen that for the DT + Ge system, when the concentration of Ge is less than 5%, the third-order nonlinear effect cannot be ignored. In other words, the linear response term $\sim \alpha_1 \xi_{\text{Ge}}$ cannot perfectly describe the physical dependence mechanism of η on ξ_{Ge} . This is very different from DT + C and DT + Si systems. The maximal change ratio reaches $\sim 44\%$ ($\sim 53\%$) when the temperature is 5 keV (10 keV), which is much larger than those of DT + C and DT + Si plasmas. The corresponding linear coefficient α_1 and nonlinear coefficients α_2 and α_3 are listed in the Table I, from which we can see that α_1 and (negative) α_3 decrease while α_2 increases as the density of DT is increased. Especially, α_1 becomes negative when the density of DT is larger than 300 g/cm³ and the temperature is 5 keV.

Following the same way used above, we also calculate the change ratio of deposition depth χ induced by Ge mixed into DT plasmas, and typical results of χ for three densities of DT that $\rho_T = 10, 100, \text{ and } 500 \text{ g/cm}^3$ are presented in

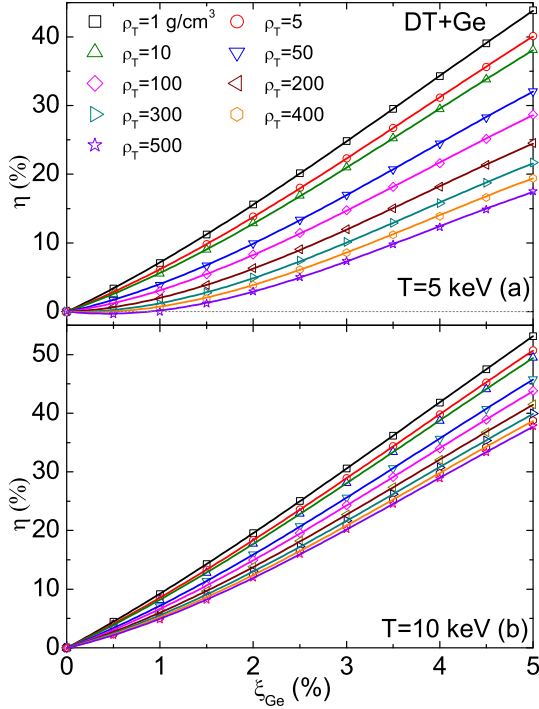


FIG. 7. Change ratio of stopping power of DT + Ge plasmas to α particle as a function of the Ge-mixing concentration ξ_{Ge} . All other parameters are the same as those used in Fig. 3.

Fig. 8. We will not show the results for other densities for brevity. Same as the behavior of the stopping power, third-order nonlinear response of χ to ξ_{Ge} is also of importance, which can be clearly seen from Fig. 8. The data of coefficients $\gamma_{1,2,3}$ are shown in Table II. The dependence of $\gamma_{1,2,3}$ on the density of DT is the same as the dependence of $\alpha_{1,2,3}$ on the density of DT. In addition, the maximal change ratio of deposition depth induced by Ge reaches about 40% much larger than those induced by C and Si.

IV. DISCUSSIONS

As a consequence, the higher the atomic number of impurities mixed into DT plasmas, the more remarkable the changes of stopping power and deposition depth of charged particles, and the more significant the nonlinear response of the change ratios (η and χ) to the impurity concentration (ξ_X). This nonlinear effect indicates that the long-range classical collision contribution may be much stronger for the impurities with higher ionization and heavier atomic mass. However, based on the systematic investigations and discussions above, we can determine that the linear response behaviors of η and χ to ξ_X is the simplest and the most important.

As a theoretical study of the effect of impurity mixing on the stopping power, it should be perfectly reasonable for us to choose the highest impurity concentration of 5%, but we emphasize that the highest mix cases are extreme examples. From the point of view of energy deposition of charged particles, the impurity elements mixed in DT hot spot will significantly reduce the deposition radius of α particle, which is conducive

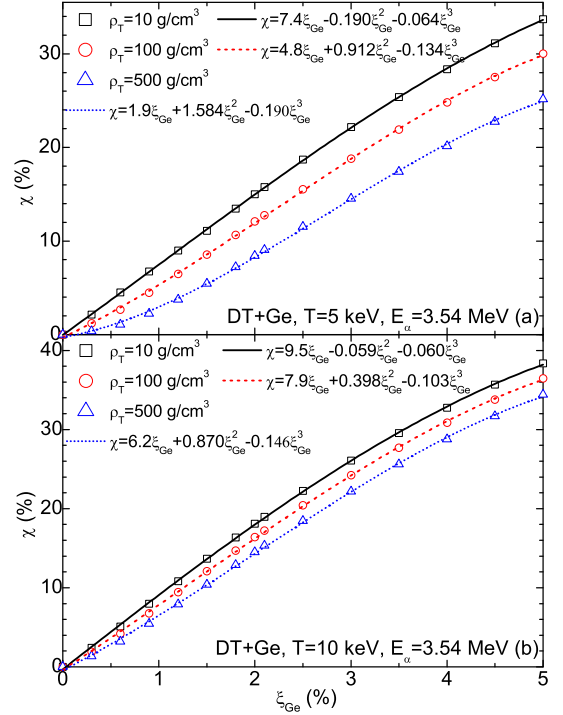


FIG. 8. Change ratio of deposition depth of α -particle moving in DT + Ge plasmas as a function of the Ge-mixing concentration ξ_{Ge} . Here we just show the results for three different densities $\rho_T = 10, 100, \text{ and } 500 \text{ g/cm}^3$. All other parameters are the same as those used in Fig. 4.

to the temperature rise of hot spot, and ultimately achieve ignition. However, from the perspective of the radiation hydrodynamic, the incorporation of excessive high-Z elements (such as CH, Si-doped CH, and Ge-doped CH from the shell ablator) may radiatively cool the DT hot spot, reducing the ion temperature and decreasing the neutron yield. For example, following the formula in Ref. [31], at $\sim 5\%$ atomic mix and assuming that the free-free emissivity scales like Z^2 , one would expect increases in radiative loss from the fuel from a factor of ~ 3 (for C) to ~ 135 (for Ge). These are high numbers compared to the most mixed experimental cases in Ref. [31], which is worth noting. Therefore, in the actual design study of the ICF layered target with an ablator composed of a high-Z material, an appropriate impurity concentration is crucial. At present, the level of ablator impurities mixed into DT hot spots can be determined quantitatively by using the experimentally measured level of elevated x-ray emission to neutron yield of the hot spot combined with corresponding theoretical models [31].

The analysis in this paper is based on the BPS model, which is only applicable to weakly coupled plasmas. In other words, our formula can be applied to the case where the plasma coupling strength is less than unity. In the above calculations of DT + X ($X = \text{C, Si, Ge}$) plasmas, we considered the temperature of the system from $\sim 5 \text{ keV}$ to $\sim 10 \text{ keV}$. This temperature range should be what we expect to find in the center of an ICF hot spot. As shown in Fig. 1, this temperature range ensures that the plasma is in the weakly coupled region. Previous experimental studies have shown that much of the

effects of α -heating occur at the hot-spot edge and in the cold fuel layer, where the plasma temperature is about ~ 500 eV to ~ 5 keV. From the above results, such as Fig. 7 and Fig. 8, it can be seen that at lower temperature (i.e., $T = 5$ keV), the nonlinear response of α -particle energy deposition to impurity concentration seems to be more obvious when the middle and high Z element (such as Ge) is mixed. It is clear to us that the lower the plasma temperature, the greater the plasma coupling strength. Conversely, the lower the temperature, the lower the ionization of the plasma X ($X = C, Si, Ge$). Therefore, these factors should be treated very carefully when the formulas developed in this article are applied to lower-temperature plasma states, especially when applied to ICF target design. As long as the plasma is in a weakly coupled state (i.e., $g_p < 1$), the formulas for impurity effects in this paper should be applicable.

In order to illustrate this point more clearly, as an example, here we further calculated the case of DT + X ($X = C, Si, Ge$) where the temperature of DT is ~ 2 keV, the mass density of DT is ~ 100 g/cm³, and the maximum mixing concentration of X is still $\sim 5\%$. We emphasize that in this plasma state, the ionization degrees of C, Si, and Ge are nearly $Z_C^* \approx 5.9$, $Z_{Si}^* \approx 13.8$, and $Z_{Ge}^* \approx 29.0$, respectively. It is clear that C and Si are almost completely ionized, while Ge is partially ionized. For such weakly coupled plasmas of partial ionization, our formulas are still applicable. It is only necessary to substitute the effective ionization degree into the above formulas to complete the corresponding calculations. The overall plasma coupling strengths are less than unity. Explicitly, the maximum values of g_p are about $\sim 8.8 \times 10^{-2}$, $\sim 2.7 \times 10^{-1}$, and $\sim 7.0 \times 10^{-1}$ for DT + C, DT + Si, and DT + Ge plasmas, respectively. The calculations found that (i) for the DT + C plasmas, the change ratio of stopping power η is linear response to the mixing concentration of C ξ_C by a relationship that $\eta = 1.4\xi_C + O(\xi_C^2)$; (ii) for the DT + Si plasmas, the second-order nonlinear effect cannot be ignored and $\eta = 1.4\xi_{Si} + 0.065\xi_{Si}^2 + O(\xi_{Si}^3)$; and (iii) for the DT + Ge plasmas, higher-order nonlinear effect is observed and $\eta = \sum_{i=1}^4 \alpha_i \xi_{Ge}^i + O(\xi_{Ge}^5)$ with the linear response coefficient $\alpha_1 = -4.73$, and the nonlinear coefficients $\alpha_2 = 2.73$, $\alpha_3 = -0.46$, and $\alpha_4 = 0.03$. Comparing with the data in Table I, it is not difficult to find that when the temperature is ~ 2 keV, the nonlinear effect will be more significant for DT + Ge plasmas. For brevity, we will not discuss other lower-temperature situations in detail.

In our work, the theoretical analysis and prediction of the effect of impurity mixing on the energy deposition of charged particles are of scientific significance in the application of BPS model, and the theoretical findings herein have never been reported in previous literatures. With the significant development of energy deposition experimental technology in the world, the concentration of impurity elements mixed into DT hot spots may be measured quantitatively through experimental studies of energy deposition of charged particles. The nonlinear response of energy deposition of charged particles caused by the incorporation of impurity elements may be also observed by excellent energy loss related experiments in future. At present, experimental studies on the energy deposition of the charged particles in dense plasma focuses on the appropriation of relevant theoretical models near the Bragg peak of the stopping power [26–30]. Our work

provides more innovative ideas, as well as useful theoretical basis and data support for experimental scientists to carry out relevant experimental research in future. This will be of interest and importance, and has the value of scientific research, which is beneficial to the actual design research of ICF target.

Before ending this paper, we would like to point out that the stopping power per unit areal density [15] $\frac{dE}{d(\rho R)}$ show the same effect due to the change in density. Same as Eq. (32), the change ratio of the total stopping power per unit areal density $\frac{dE}{d(\rho R)}$ due to the mixing of X is given by $\eta' = \frac{\frac{dE}{d(\rho R)} - \frac{dE_0}{d(\rho R)}}{\frac{dE_0}{d(\rho R)}}$, where $\frac{dE_0}{d(\rho R)}$ is the stopping power without mixing of X . By employing the relationships that $\rho_X = m_X \xi_X n_T$, $\rho_D = \rho_T$, and $\rho = \rho_X + \rho_D + \rho_T$, we could easily get that

$$\eta' = \frac{2m_T}{2m_T + m_X \xi_X} \eta - \frac{m_X \xi_X}{2m_T + m_X \xi_X}. \quad (49)$$

In the limit of lower mixing concentration, i.e., $\xi_X \rightarrow 0$, we have

$$\eta' = \left(\alpha_1 + \frac{m_X}{2m_T} \right) \xi_X + \left(\alpha_2 - \frac{m_X}{2m_T} \alpha_1 - \frac{m_X^2}{4m_T^2} \right) \xi_X^2 + \left(\alpha_3 - \frac{m_X}{2m_T} \alpha_2 + \frac{m_X^2}{4m_T^2} \alpha_1 + \frac{m_X^3}{8m_T^3} \right) \xi_X^3 + \dots, \quad (50)$$

where Eq. (33) has been used. The change ratio of the total stopping power per unit areal density also presents linear and nonlinear response behavior to the concentration ξ_X , but the response coefficients are modified compared with Eq. (33) which casts in terms of the path-length quantity (i.e., dE/dx). For instances, comparing Eq. (33) with Eq. (50), the linear response coefficient to ξ_X is modified from α_1 to $\alpha_1 + \frac{m_X}{2m_T}$; the second-order nonlinear coefficient is modified from α_2 to $\alpha_2 - \frac{m_X}{2m_T} \alpha_1 - \frac{m_X^2}{4m_T^2}$; and the third-order nonlinear coefficient is modified from α_3 to $\alpha_3 - \frac{m_X}{2m_T} \alpha_2 + \frac{m_X^2}{4m_T^2} \alpha_1 + \frac{m_X^3}{8m_T^3}$. We will not discuss it in more detail for brevity.

V. CONCLUSIONS

In conclusion, we have studied the influence of the impurities mixed into hot dense DT plasmas on the energy loss of charged particle deposited therein by employing the BPS model. We have carefully derived the analytical expressions for the change ratios of stopping power and the deposition depth of charged particles induced by impurities in DT plasmas. The change ratios of both classical short-distance collision and quantum correction contributions linearly depend on the impurity concentration ξ_X . While the change ratio of classical long-range collision contribution includes higher-order nonlinear responses to ξ_X . The explicit expressions for the linear and nonlinear response coefficients have been obtained. Furthermore, we have also derived the expression for change ratio of deposition depth of charged particles induced by impurities in DT plasmas. Combined the analytical analysis and numerical simulations, we have

systemically studied the stopping power of hot dense DT plasmas mixed with impurity X ($X = \text{C}, \text{Si}, \text{Ge}$) to α particles within high incident velocity. We have found that when C is mixed into DT, both change ratios of stopping power and deposition depth of α particles (i.e., η and χ) are linear response to the concentration of C ξ_C ; while if Si (Ge) is mixed into DT, the second- (and even third-) order nonlinear responses of η and χ to ξ_{Si} (ξ_{Ge}) becomes significant. This nonlinear effect is resulted from the higher ionization degrees and heavier atomic masses of Si and Ge. We hope that our findings and analysis in this work will be helpful to the research of ICF related implosion physics and provide useful theoretical guidance and data for the design of ICF target.

ACKNOWLEDGMENTS

This work was supported by the National Key R&D Program of China under Grant No. 2017YFA0403200; by the Science Challenge Project of China Academy of Engineering Physics (CAEP) under Grant No. TZ2016001; by the National Natural Science Foundation of China (NSFC) under Grants No. 11675023, No. 11625415, No. 11575032, No. 11675024, and No. 11947202; by the NSFC-NSAF under Grant No. U1530258; by the Innovation Development Foundation of CAEP under Grant No. ZYCX1921-02; by the Presidential Foundation of CAEP under Grant No. YZ2015014; and by the China Postdoctoral Science Foundation under Grant No. 2019M660016.

-
- [1] S. H. Glenzer, B. J. MacGowan, P. Michel, N. B. Meezan, L. J. Suter, S. N. Dixit, J. L. Kline, G. A. Kyrala, D. K. Bradley, D. A. Callahan *et al.*, Symmetric inertial confinement fusion implosions at ultra-high laser energies, *Science* **327**, 1228 (2010).
- [2] C. K. Li, F. H. Sëguin, J. A. Frenje, M. Rosenberg, R. D. Petrasso, P. A. Amendt, J. A. Koch, O. L. Landen, H. S. Park, H. F. Robey *et al.*, Charged-particle probing of x-ray-driven inertial-fusion implosions, *Science* **327**, 1231 (2010).
- [3] J. A. Frenje, C. K. Li, F. H. Sëguin, D. T. Casey, R. D. Petrasso, D. P. McNabb, P. Navratil, and S. Quaglioni, T. C. Sangster, V. Y. Glebov, and D. D. Meyerhofer, Measurements of the Differential Cross Sections for the Elastic $n\text{-H}3$ and $n\text{-H}2$ Scattering at 14.1 MeV by using an Inertial Confinement Fusion Facility, *Phys. Rev. Lett.* **107**, 122502 (2011).
- [4] T. Döppner, C. A. Thomas, L. Divol, E. L. Dewald, P. M. Celliers, D. K. Bradley, D. A. Callahan, S. N. Dixit, J. A. Harte, S. M. Glenn *et al.*, Direct Measurement of Energetic Electrons Coupling to an Imploding Low-Adiabatic Inertial Confinement Fusion Capsule, *Phys. Rev. Lett.* **108**, 135006 (2012).
- [5] S. P. Regan, R. Epstein, B. A. Hammel, L. J. Suter, H. A. Scott, M. A. Barrios, D. K. Bradley, D. A. Callahan, C. Cerjan, G. W. Collins *et al.*, Hot-Spot Mix in Ignition-Scale Inertial Confinement Fusion Targets, *Phys. Rev. Lett.* **111**, 045001 (2013).
- [6] D. Wu, X. T. He, W. Yu, and S. Fritzsche, Monte Carlo approach to calculate proton stopping in warm dense matter within particle-in-cell simulations, *Phys. Rev. E* **95**, 023207 (2017).
- [7] J. Frank, A. King, and D. Raine, *Accretion Power in Astrophysics* (Cambridge University Press, Cambridge, 2002).
- [8] M. W. C. Dharma-wardana, Quantum Corrections and Bound-State Effects in the Energy Relaxation of Hot Dense Hydrogen, *Phys. Rev. Lett.* **101**, 035002 (2008).
- [9] M. D. Barriga-Carrasco, Dynamical local field corrections on energy loss in plasmas of all degeneracies, *Phys. Rev. E* **79**, 027401 (2009).
- [10] Z.-G. Fu, Z. Wang, and P. Zhang, Energy loss of α -particle moving in warm dense deuterium plasma: Role of local field corrections, *Phys. Plasmas* **24**, 112710 (2017).
- [11] Z.-G. Fu, Z. Wang, M.-L. Li, D.-F. Li, W. Kang, and P. Zhang, Dynamic properties of the energy loss of multi-MeV charged particles traveling in two-component warm dense plasmas, *Phys. Rev. E* **94**, 063203 (2016).
- [12] C. K. Li and R. D. Petrasso, Charged-Particle Stopping Powers in Inertial Confinement Fusion Plasmas, *Phys. Rev. Lett.* **70**, 3059 (1993).
- [13] L. S. Brown, D. L. Preston, and R. L. Singleton Jr., Charged particle motion in a highly ionized plasma, *Phys. Rep.* **410**, 237 (2005).
- [14] R. L. Singleton, Jr., Charged particle stopping power effects on ignition: Some results from an exact calculation, *Phys. Plasmas* **15**, 056302 (2008).
- [15] M. Mahdavi, and T. Koohrokhi, Energy deposition of multi-MeV protons in compressed targets of fast-ignition inertial confinement fusion, *Phys. Rev. E* **85**, 016405 (2012).
- [16] J. Daligault, On the quantum Landau collision operator and electron collisions in dense plasmas, *Phys. Plasmas* **23**, 032706 (2016).
- [17] J. Daligault, Collisional transport coefficients of dense high-temperature plasmas within the quantum Landau-Fokker-Planck framework, *Phys. Plasmas* **25**, 082703 (2018).
- [18] P. E. Grabowski, M. P. Surh, D. F. Richards, F. R. Graziani, and M. S. Murillo, Molecular Dynamics Simulations of Classical Stopping Power, *Phys. Rev. Lett.* **111**, 215002 (2013).
- [19] A. Schleife, Y. Kanai, and A. A. Correa, Accurate atomistic first-principles calculations of electronic stopping, *Phys. Rev. B* **91**, 014306 (2015).
- [20] A. A. Shukri and F. Bruneval, *Ab initio* electronic stopping power of protons in bulk materials, *Phys. Rev. B* **93**, 035128 (2016).
- [21] Y. H. Ding, A. J. White, S. X. Hu, O. Certik, and L. A. Collins, *Ab initio* Studies on the Stopping Power of Warm Dense Matter with Time-Dependent Orbital-Free Density Functional Theory, *Phys. Rev. Lett.* **121**, 145001 (2018).
- [22] A. J. White, O. Certik, Y. H. Ding, S. X. Hu, and L. A. Collins, Time-dependent orbital-free density functional theory for electronic stopping power: Comparison to the Mermin-Kohn-Sham theory at high temperatures, *Phys. Rev. B* **98**, 144302 (2018).
- [23] I. Maliyov, J.-P. Crocombette, and F. Bruneval, Electronic stopping power from time-dependent density-functional theory in Gaussian basis, *Eur. Phys. J. B* **91**, 172 (2018).

- [24] N. Schlünzen, K. Balzer, M. Bonitz, L. Deuchler, E. Pehlke, Time-dependent simulation of ion stopping: Charge transfer and electronic excitations, *Contrib. Plasma Phys.* **59**, e201800184 (2019).
- [25] C. F. Clauser and N. R. Arista, Stopping power of dense plasmas: The collisional method and limitations of the dielectric formalism, *Phys. Rev. E* **97**, 023202 (2018).
- [26] J. A. Frenje, P. E. Grabowski, C. K. Li, F. H. Séguin, A. B. Zylstra, M. Gatu Johnson, R. D. Petrasso, V. Y. Glebov, and T. C. Sangster, Measurements of Ion Stopping Around the Bragg Peak in High-Energy-Density Plasmas, *Phys. Rev. Lett.* **115**, 205001 (2015).
- [27] W. Cayzac, A. Frank, A. Ortner, V. Bagnoud, M. M. Basko, S. Bedacht, C. Bläser, A. Blažević, S. Busold, O. Deppert *et al.*, Experimental discrimination of ion stopping models near the Bragg peak in highly ionized matter, *Nat. Commun.* **8**, 15693 (2017).
- [28] J. A. Frenje, R. Florido, R. Mancini, T. Nagayama, P. E. Grabowski, H. Rinderknecht, H. Sio, A. Zylstra, M. G. Johnson, C. K. Li, F. H. Séguin, R. D. Petrasso, V. Yu Glebov, and S. P. Regan, Experimental Validation of Low-Z Ion-Stopping Formalisms Around the Bragg Peak in High-Energy-Density Plasmas, *Phys. Rev. Lett.* **122**, 015002 (2019).
- [29] A. B. Zylstra, J. A. Frenje, P. E. Grabowski, C. K. Li, G. W. Collins, P. Fitzsimmons, S. Glenzer, F. Graziani, S. B. Hansen, S. X. Hu *et al.*, Measurement of Charged-Particle Stopping in Warm Dense Plasma, *Phys. Rev. Lett.* **114**, 215002 (2015).
- [30] D. B. Sayre, C. J. Cerjan, S. M. Sepke, D. O. Gericke, J. A. Caggiano, L. Divol, M. J. Eckart, F. R. Graziani, G. P. Grim, S. B. Hansen *et al.*, Neutron Time-of-Flight Measurements of Charged-Particle Energy Loss in Inertial Confinement Fusion Plasmas, *Phys. Rev. Lett.* **123**, 165001 (2019).
- [31] T. Ma, P. K. Patel, N. Izumi, P. T. Springer, M. H. Key, L. J. Atherton, L. R. Benedetti, D. K. Bradley, D. A. Callahan, P. M. Celliers *et al.*, Onset of Hydrodynamic Mix in High-Velocity, Highly Compressed Inertial Confinement Fusion Implosions, *Phys. Rev. Lett.* **111**, 085004 (2013).
- [32] O. A. Hurricane, D. A. Callahan, D. T. Casey, E. L. Dewald, T. R. Dittrich, T. Döppner, M. A. Berrios Garcia, D. E. Hinkel, L. F. Berzak Hopkins, P. Kervin *et al.*, The high-foot implosion campaign on the National Ignition Facility, *Phys. Plasmas* **21**, 056314 (2014).
- [33] M. Lafon and M. Bonnefille, Stabilization of thin-shell implosions using a high-foot adiabat-shaped drive at the National Ignition Facility, *Phys. Plasmas* **25**, 102708 (2018).
- [34] R. E. Olson, G. A. Rochau, O. L. Landen, and R. J. Leeper, X-ray ablation rates in inertial confinement fusion capsule materials, *Phys. Plasmas* **18**, 032706 (2011).
- [35] S. P. Regan, R. Epstein, B. A. Hammel, L. J. Suter, J. Ralph, H. Scott, M. A. Barrios, D. K. Bradley, D. A. Callahan, C. Cerjan *et al.*, Hot-spot mix in ignition-scale implosions on the NIF, *Phys. Plasmas* **19**, 056307 (2012).
- [36] L. F. Berzak Hopkins, S. Le Pape, L. Divol, N. B. Meezan, A. J. Mackinnon, D. D. Ho, O. S. Jones, S. Khan, J. L. Milovich, J. S. Ross *et al.*, Near-vacuum hohlraums for driving fusion implosions with high density carbon ablaters, *Phys. Plasmas* **22**, 056318 (2015).
- [37] L. F. Berzak Hopkins, N. B. Meezan, S. Le Pape, L. Divol, A. J. Mackinnon, D. D. Ho, M. Hohenberger, O. S. Jones, G. Kyrala, J. L. Milovich *et al.*, First High-Convergence Cryogenic Implosion in a Near-Vacuum Hohlraum, *Phys. Rev. Lett.* **114**, 175001 (2015).
- [38] N. B. Meezan, L. F. Berzak Hopkins, S. Le Pape, L. Divol, A. J. MacKinnon, T. Döppner, D. D. Ho, O. S. Jones, S. F. Khan, T. Ma *et al.*, Cryogenic tritium-hydrogen-deuterium and deuterium-tritium layer implosions with high density carbon ablaters in near-vacuum hohlraums, *Phys. Plasmas* **22**, 062703 (2015).
- [39] S. Le Pape, L. F. Berzak Hopkins, L. Divol, N. Meezan, D. Turnbull, A. J. Mackinnon, D. Ho, J. S. Ross, S. Khan, A. Pak *et al.*, The near vacuum hohlraum campaign at the NIF: A new approach, *Phys. Plasmas* **23**, 056311 (2016).
- [40] O. L. Landen, T. R. Boehly, D. K. Bradley, D. G. Braun, D. A. Callahan, P. M. Celliers, G. W. Collins, E. L. Dewald, L. Divol, S. H. Glenzer *et al.*, Capsule performance optimization in the National Ignition Campaign, *Phys. Plasmas* **17**, 056301 (2010).
- [41] Z. Wang, Z.-G. Fu, B. He, and P. Zhang, Energy relaxation of multi-MeV protons traveling in compressed DT+ Be plasmas, *Phys. Plasmas* **21**, 072703 (2014).
- [42] Z. Wang, Z.-G. Fu, and P. Zhang, Theoretical studies on the stopping power of deuterium-tritium mixed with uranium plasmas for α particles, *Phys. Plasmas* **21**, 102307 (2014).
- [43] S. B. Hansen, A. Y. Faenov, T. A. Pikuz, K. B. Fournier, R. Shepherd, H. Chen, K. Widmann, S. C. Wilks, Y. Ping, and H. K. Chung *et al.*, Temperature determination using $K\alpha$ spectra from M -shell Ti ions, *Phys. Rev. E* **72**, 036408 (2005).
- [44] V. A. Smalyuk, L. J. Atherton, L. R. Benedetti, R. Bionta, D. Bleuel, E. Bond, D. K. Bradley, J. Caggiano, D. A. Callahan, D. T. Casey *et al.*, Performance of High-Convergence, Layered DT Implosions with Extended-Duration Pulses at the National Ignition Facility, *Phys. Rev. Lett.* **111**, 215001 (2013).